Monthly Notices of the ROYAL ASTRONOMICAL SOCIETY
MNRAS **508,** 1156–1164 (2021) https://doi.org/10.1093/mnras/stab2620
Advance Access publication 2021 September 20

The search for failed supernovae with the Large Binocular Telescope: N6946-BH1, still no star

C. M. Basinger,[1★] C. S. Kochanek,[1,2] S. M. Adams ,[3] X. Dai[4] and K. Z. Stanek[1,2]
[1]*Department of Astronomy, The Ohio State University, 140 West 18th Avenue, Columbus, OH 43210, USA*
[2]*Center for Cosmology and AstroParticle Physics (CCAPP), The Ohio State University, 191 W. Woodruff Avenue, Columbus, OH 43210, USA*
[3]*The Aerospace Corporation, Chantilly, VA 20151, USA*
[4]*Department of Physics and Astronomy, University of Oklahoma, 440 W. Brooks Street, Norman, OK 73019, USA*

Accepted 2021 September 4. Received 2021 July 27; in original form 2020 July 31

ABSTRACT
We present new Large Binocular Telescope, *Hubble Space Telescope*, and *Spitzer Space Telescope* data for the failed supernova candidate N6946-BH1. We also report an unsuccessful attempt to detect the candidate with *Chandra*. The $\sim$300 000 $L_\odot$ red supergiant progenitor underwent an outburst in 2009 and has since disappeared in the optical. In the LBT data from 2008 May through 2019 October, the upper limit on any increase in the R-band luminosity of the source is 2000 $L_\odot$. *HST* and *Spitzer* observations show that the source continued to fade in the near-IR and mid-IR, fading by approximately a factor of 2 between 2015 October and 2017 September to 2900 $L_\odot$ at H band (*F160W*). Models of the spectral energy distribution are inconsistent with a surviving star obscured either by an ongoing wind or dust formed in the transient. The disappearance of N6946-BH1 remains consistent with a failed supernova, but the post-failure phenomenology requires further theoretical study.

Key words: black hole physics – stars: massive.

1 INTRODUCTION

In modern theoretical models of supernovae (SNe), it is expected that some 10–30 per cent of core collapses fail to lead to an SNe and instead become black holes (e.g. O'Connor & Ott 2011; Pejcha & Thompson 2015; Sukhbold et al. 2016) with a weaker intermediate transient (Lovegrove & Woosley 2013). Fall back SNe, where a successful SN explosion falls back on to the proto-neutron star and leads to black hole formation, are expected to be very rare (Sukhbold et al. 2016). The existence of failed SNe naturally explains both the apparent lack of higher mass progenitors to red supergiants (Kochanek et al. 2008; Smartt et al. 2009) and the compact object mass function (Kochanek 2014a, 2015).

From observations of interacting black hole binaries (McClintock & Remillard 2006) and non-interacting binaries (Thompson et al. 2019), as well as LIGO (e.g. Abbott et al. 2016), we know that stellar mass black holes exist. However, the mass distribution of black holes inferred from interacting binaries and merging systems is intrinsically biased (e.g. Belczynski et al. 2016), and tells us nothing of the parent populations of stars which produced these black holes. There is basically no prospect of existing or next generation neutrino or gravitational wave detectors observing the formation of a new black hole (see Adams et al. 2013). This leaves surveys like that proposed by Kochanek et al. (2008) as the only current prospect of directly investigating the formation of black holes.

In Kochanek et al. (2008), we proposed a search for failed SNe by looking for massive stars that 'vanish'. We reported first results and a first candidate N6946-BH1 in Gerke, Kochanek & Stanek (2015), with follow-up observations of the candidate in Adams et al. (2017a) and updated statistics in Adams et al. (2017b). The implied SN rates and the properties of the candidate were both consistent with expectations.

There is no doubt that the progenitor of N6946-BH1 was a massive luminous star that subsequently vanished in the optical and has at best a much fainter and fading near-IR counterpart. The absence of a warm-*Spitzer* counterpart implies that the star cannot be obscured by a present-day, dusty wind. Newly forming dust is hot, leading to visible near/mid-IR emission unless the optical depths are very high. This leaves only the possibility of obscuration by dust formed during the transient associated with the vanishing of the star.

Ideally, we would test this hypothesis with *James Webb Space Telescope* (*JWST*) observations at 10–20 μm to search for the mid-IR dust emission required by this hypothesis, and this remains a future prospect. However, time will also tell. A required feature of any model obscuring the progenitor with an expanding shell of dust is that the star must eventually reappear. The optical depth of an expanding continuous shell of any shape decreases as t^{-2} and any evolution of the shell to be inhomogeneous accelerates the rate of decline by creating lower optical depth channels through which light escapes more easily (Kochanek, Szczygieł & Stanek 2012). It is important to understand that this minimal t^{-2} evolution is simply a consequence of expansion and mass conservation and is not restricted to the spherical models we use below. If we divide the sky into patches of solid angle $\Delta\Omega_i$ and eject mass M_i at velocity v_i into each patch, mass conservation requires $M_i = \Sigma_i R^2 \Delta\Omega_i$ at radius R, so the mean surface density of each patch evolves as $\Sigma_i \propto R^{-2} \propto v_i^{-2} t^{-2} \propto t^{-2}$ once the velocity is constant or slowly evolving. Differentially varying the solid angles with time or using velocity fields that do not maintain a fairly uniform global shell correspond to clumping,

★ E-mail: basinger.101@osu.edu

which, as already noted, will accelerate the evolution to be faster than t^{-2}.

It is clear that a star with the properties of the progenitor is no longer present. There are no existing models for why the properties of a surviving star would be wildly different than the progenitor, with one exception. The surviving companion of a single-degenerate Type Ia SN is overluminous (e.g. Shappee, Kochanek & Stanek 2013). Most of the mass lost by the surviving companion is from ablation due to shock heating of the envelope. This leaves a star with an inflated envelope that is cooler and more luminous for 10^3-10^4 yr due to Kelvin–Helmholtz contraction. Despite the lack of any models beyond this analogue to Type Ia companions, in Adams et al. (2017a) and this paper we consider stars of any temperature and luminosity that fit our SEDs.

In Adams et al. (2017a), we reported on continued Large Binocular Telescope (LBT) observations of N6946-BH1 through the end of 2015 along with *Hubble Space Telescope* (*HST*) *F606W* (V), *F814W* (I), *F110W* (J), and *F160W* (H) band observations. In the LBT data, we could see no evidence for any late-time brightening or fading of the source in the *U*, *B*, *V*, and *R* bands. In the optical *HST* bands, the star had effectively vanished, but there did seem to be a faint, fading near-IR counterpart whose luminosity was consistent with some models (e.g. Perna et al. 2014) for late-time accretion on to a newly formed black hole. While the rate of decline in the luminosity is consistent with the existence of an accretion disc, Fernández et al. (2018) found it surprising that we observed the luminosity fading on these time-scales, claiming that the bolometric luminosity should decay minimally or be roughly constant for many years.

In this paper, we extend the LBT monitoring observations through the end of 2019. We discuss new *HST J* and *H* band observations from 2017 September and a 4.5 µm *Spitzer Space Telescope* (*SST*) observation from 2018 September, roughly 2 and 3 yr after the previous observations, respectively. We still see no changes in the optical emission at the location of N6946-BH1, while the source faded in the near-IR and mid-IR. We also report an unsuccessful attempt to detect an X-ray counterpart with the *Chandra* X-ray Observatory. We discuss the data in Section 2. In Section 3, we constrain the optical variability of the source. In Section 4, we interpret the results of Sections 3 and 4 for any model with a surviving star. In Section 5, we discuss how accretion on to a newly formed black hole differs from a surviving star. We discuss the results in Section 6. We adopt the revised distance to NGC 6946 of 7.7 Mpc (Anand, Rizzi & Tully 2018) and a Galactic extinction of $E(B-V)=0.303$ based on the Schlafly & Finkbeiner (2011) recalibration of Schlegel, Finkbeiner & Davis (1998).

2 OBSERVATIONS AND DATA

We obtained new *HST* WFPC3/IR *F110W* (*J*) and *F160W* (*H*) band images of N6946-BH1 on 2017 September 15. We obtained three dithered images in both the *J* and *H* bands, with total integration times of 1350 and 1500 s, respectively. We reduced the data using DOLPHOT (Dolphin 2000). We compare these images with *HST* Wide Field Camera 3 (WFC3) IR *J* and *H* band images from 2015 October 8, using IRAF to align the 2015 and 2017 images with a simple rotation and then using ISIS (Alard & Lupton 1998; Alard 2000) to generate difference images between the two epochs.

We do photometry on the unaltered 2017 images using DOLPHOT with the parameters and procedures described in Adams & Kochanek (2015). We use a drizzled 2007 *HST* WFPC2 *F814W* (*I*) band pre-outburst image as the astrometric reference as in Adams et al. (2017a). The 2017 images are aligned to the pre-outburst image

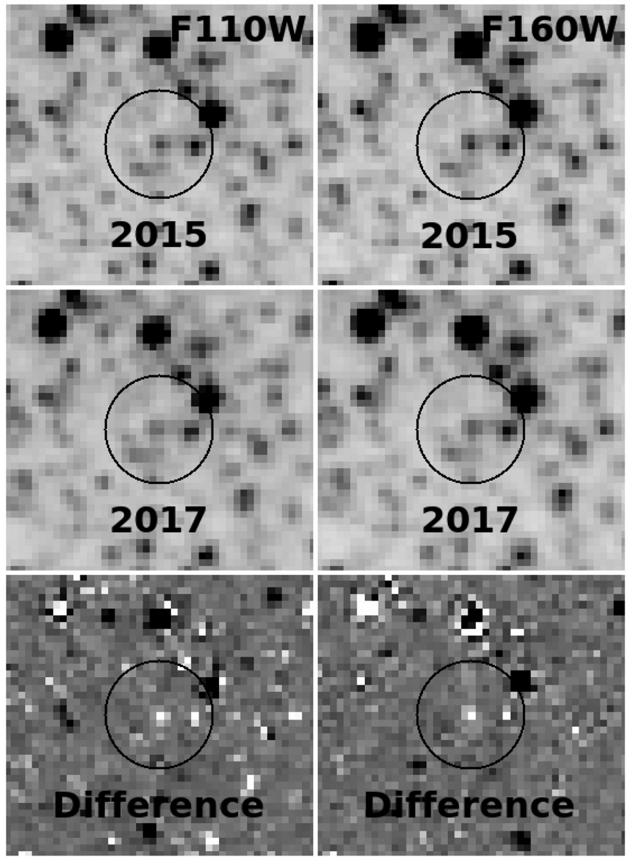

Figure 1. Near-IR *HST* images centred on the location of N6946-BH1. The top row shows the 2015 *J* (left) and *H* band (right) images. The middle row shows the corresponding 2017 images. The bottom row shows the difference images. The circles have a radius of 1 arcsec. Darker colours in all panels indicate a greater flux. The faint IR emission has faded by a factor of ∼2 from 2015 to 2017.

with TWEAKREG and TWEAKBACK from the DRIZZLEPAC package with an rms error of 0.05 arcsec. Using the pre-outburst image as the reference allows us to do photometry at the known location of the progenitor. Using the new *H* band image as the reference for photometry yields similar results. We will adopt the values obtained from the aligned images with the 2007 epoch as a reference to remain consistent with Adams et al. (2017a).

Our 2015 and 2017 WFC3-IR *J* and *H* band images of the region surrounding the candidate are shown in Fig. 1. We also show the difference between them, where black (white) indicates a source that has become brighter (fainter). The source whose position is consistent with that of the candidate appears to have faded between the two *HST* epochs by approximately 0.5 mag. The *HST* and *SST* magnitudes from observations since 2015 are shown in Table 1. The old *HST* mags are repeated here from Adams et al. (2017a). Our rederived *SST* magnitudes for 2015 agree with the values reported in Adams et al. (2017a). As a luminosity (νL_ν), the source has dropped from 2900 to 1900 $L_\odot$ at *J* band and from 4600 to 2900 $L_\odot$ at *H* band. Shifting the luminosity of the progenitor from Adams et al. (2017a) to the revised distance ($10^{5.29}\,L_\odot \rightarrow 10^{5.51}\,L_\odot$), these near-IR luminosities are less than 1 per cent of the luminosity of the progenitor and correspond to luminosities of 5.8 and 8.8 × $10^{-3}L_E$ relative to the Eddington luminosity L_E for a 10 $M_\odot$ black hole.

We calculate the odds of an unrelated source being detected at the same location as the progenitor as in Adams et al. (2017a).

Table 1. Photometry.

MJD	Date	Filter	Magnitude	Telescope
57303.3	2015-10-08	UVIS *F814W*	26.02 ± 0.16	*HST*
57303.3	2015-10-08	IR *F110W*	23.75 ± 0.02	*HST*
57303.3	2015-10-08	IR *F160W*	22.38 ± 0.02	*HST*
57408.2	2016-01-21	3.6 μm	18.47 ± 0.18	*SST*
57408.2	2016-01-21	4.5 μm	17.46 ± 0.09	*SST*
58011.9	2017-09-15	IR *F110W*	24.20 ± 0.03	*HST*
58011.9	2017-09-15	IR *F160W*	22.89 ± 0.04	*HST*
58381.9	2018-09-20	4.5 μm	18.01 ± 0.15	*SST*

The closest DOLPHOT source is 0.050 arcsec from the progenitor position. With a 4.2 arcsec^{-2} surface density of sources, the odds of an unrelated source being detected at the same location purely by chance is 3.2 per cent. For sources as bright as or brighter than the detection in *J* band, the surface density is 0.76 arcsec^{-2} and the likelihood is 0.6 per cent. For the detection in *H* band, the surface density is 0.64 arcsec^{-2} and the likelihood is 0.5 per cent.

We incorporate new channel 2 (4.5 μm) *SST* data from 2018 September 20 (program ID: 13239; PI: K. Krafton) in addition to archival *SST* data into our analysis. We do aperture photometry following Adams et al. (2017a), using a 2.4 arcsec aperture and 2.4–4.8 arcsec radius sky annulus (Table 1). We use the 3.6 and 4.5 μm aperture corrections from table 4.7 of the IRAC Instrument Handbook.[1] We note that the source sits in a crowded field on a ridge of mid-IR emission, so the absolute mid-IR flux is effectively unknown. Only changes in the mid-IR flux can be reliably measured. We observe that the most recent mid-IR flux is now below its minimum value in all previous epochs.

The LBT data for NGC 6946 used here consists of 42 UBVR epochs taken from 2008 May 3 through 2019 October 24. We used the IRAF MSCRED package for data reduction and ISIS for photometry and generating light curves. The reference images used are identical to Adams et al. (2017a), and they were generated using the best ∼ 20 per cent of the data from the first 6 yr of the survey.

We extracted light curves both at the position of N6946-BH1 and for a comparison sample (Figs 2 and 3). Our comparison sample is a grid of 12 points surrounding N6946-BH1 with an inner grid spacing of 7 pixels and an outer grid spacing of 15 pixels as in Johnson, Kochanek & Adams (2017). The pixel scale is 0.2255 arcsecpixel^{-1}, so the comparison sample probes the space within several arcseconds of the candidate. Three of the twelve points in the comparison sample were eliminated due to their proximity to variable stars. We flag 'low-quality' data, defined by seeing $>1\farcs5$ or an ISIS flux scaling factor <0.8, as in Johnson et al. (2017). A low flux scaling factor indicates that the image was taken through clouds or at a high airmass.

We observed N6946-BH1 with ACIS-S3 (Garmire et al. 2003) onboard the *Chandra* X-ray Observatory (Weisskopf et al. 2002) on 2016 September 28 with an exposure time of 58.6 ks. We analysed the level 2 event files from the standard pipeline products distributed from the *Chandra* X-ray Center, where the events were filtered using the standard *ASCA* grades of 0, 2, 3, 4, and 6, good flight time intervals, and status flags. We did not detect the X-ray counterpart of the failed SN, and set 90 per cent confidence upper limits on the count rate as 5.1×10^{-5} ct s^{-1} in the full 0.5–7 keV band, and 6.1, 3.9, and 3.9×10^{-5} ct s^{-1} in the 0.5–1.2, 1.2–2, and 2–7 keV bands using the CIAO tool aprates. Assuming a power-law spectrum with a photon index of 1.7 and adopting $N_{\rm H} = 3.9 \times 10^{21}$ cm^{-2} for the combined Galactic and host galaxy absorption to X-ray sources in NGC 6946 based on the X-ray spectral fit results of Holt et al. (2003), we obtain 90 per cent confidence unabsorbed flux upper limits of 8.1, 20.8, 2.9, and 7.1×10^{-16} erg cm^{-2} s^{-1}, in the total, soft, medium, and hard bands, respectively. Assuming a blackbody spectrum of 1 keV temperature yields similar limits on the flux of 7.4, 13.3, 2.8, and 6.7×10^{-16} erg cm^{-2} s^{-1}. Assuming a 10 $M_\odot$ black hole and a distance of 7.7 Mpc, these upper limits correspond to 1500 $L_\odot$ or $4.6 \times 10^{-3} L_{\rm E}$ for the power-law model and 1400 $L_\odot$ or $4.2 \times 10^{-3} L_{\rm E}$ for the blackbody.

If we assume that the black hole is radiating at the Eddington luminosity, we can estimate the neutral hydrogen column density, N(H), required to reduce the flux below our 5.1×10^{-5} ct s^{-1} upper limit. Using the *Chandra* Proposal Planning Toolkit PIMMS v4.10,[2] we estimate N(H) $\gtrsim 1 \times 10^{24}$cm^{-2}. This estimate does not strongly depend on whether we adopt a power law or blackbody model for the input flux. The mass required to produce this absorption is roughly $M = N(H) 4\pi R^2 m_{\rm H}$, where R is the radius of the dusty shell and $m_{\rm H}$ is the mass of hydrogen. For R $\sim 10^{16}$ cm (assuming an ejecta velocity of a few hundred km s^{-1}, see Fig. 4), we find that $\gtrsim 1\ M_\odot$ of material is required. This is small compared to the 13 $M_\odot$ hydrogen envelope ejected in the failed SN model for a $\sim 25\ M_\odot$ progenitor (Woosley, Heger & Weaver 2002), so the absence of X-rays is not surprising. If there is accretion, the absence of X-rays rules out significantly higher ejecta velocities than expected for this scenario.

3 LONG-TERM VARIABILITY AND TRENDS

Our difference imaging photometry for the candidate in the LBT UBVR images is shown in Fig. 2. The light curve of N6946-BH1 is in red and the range spanned by the light curves of the comparison sample is given by the grey-shaded region. Good data points are indicated by the black circles and 'low-quality' data points are indicated by the open circles. The *R*- and *U*-band references used for difference photometry were built without using any pre-outburst images which included the progenitor. However, the *V*- and *B*-band references did include a few such images, so we performed a correction on the *V*- and *B*-band light curves to account for this contamination. Aside from data points taken in poorer conditions, the variability seen at the location of the candidate is essentially indistinguishable from the variability at other nearby locations.

This is also illustrated in Fig. 3 where we show the *R*-band reference image, a pre-outburst image of the progenitor, and *R*-band images with the minimum (2013 December 3) and maximum (2015 April 20) post-transient fluxes. The structure of the images at the position of the candidate is no different than that at the locations used to produce the comparison sample, again consistent with the lack of any variable source corresponding to the candidate.

Table 2 characterizes the stochastic variability of N6946-BH1 using the root-mean-square (RMS) and the ISIS noise estimate, $\langle \sigma^2 \rangle^{1/2}$, of the post-outburst light curves. The average RMS for the comparison sample and the standard deviation about this average are reported under the first 'Sample' column. The RMS tends to be about twice as large as the ISIS noise estimate. Since the ISIS noise estimate only considers Poisson statistics, this number is not surprising, and the comparison sample RMS is likely a better indicator of the limits on any potential variability. The RMS for N6946-BH1 is consistent with the RMS of the comparison sample except for the *V* band, which

[1] https://irsa.ipac.caltech.edu/data/SPITZER/docs/irac/iracinstrumenthandbook/

[2] https://cxc.harvard.edu/toolkit/pimms.jsp

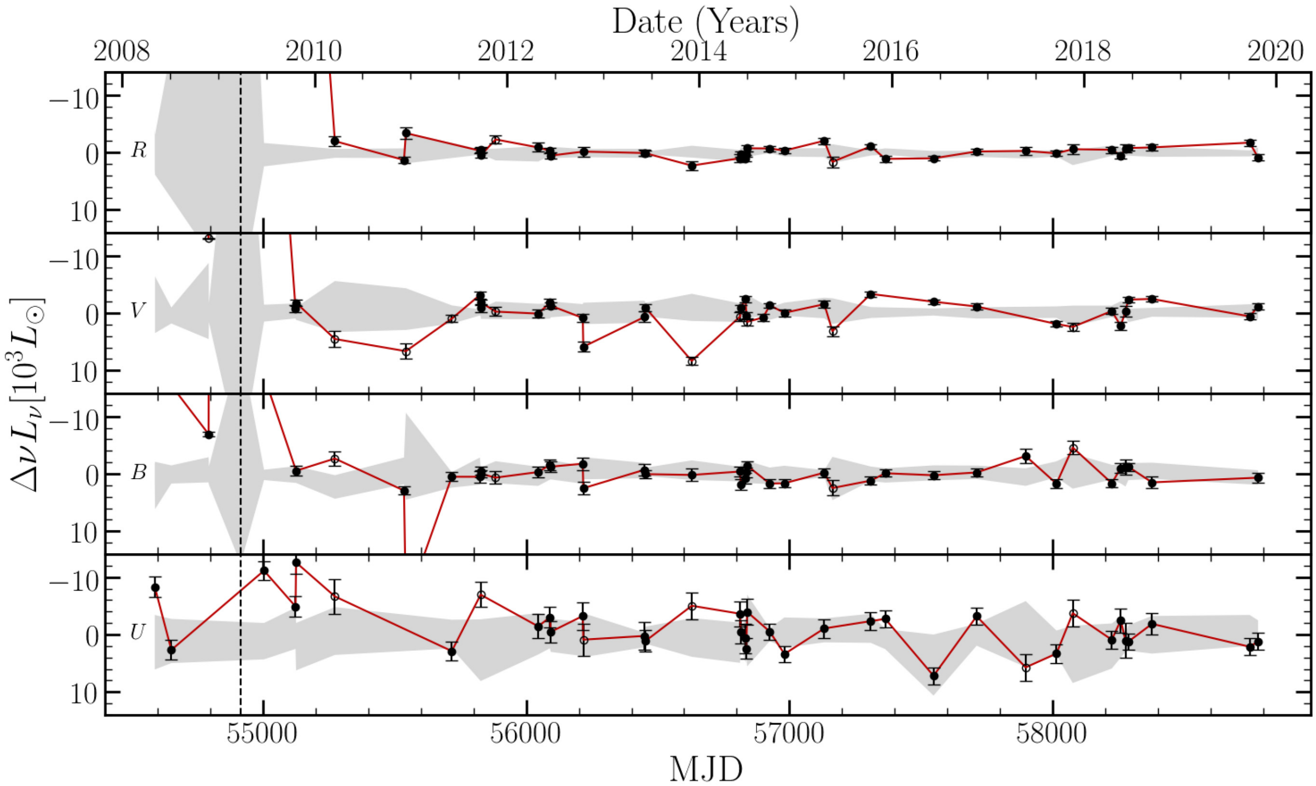

Figure 2. The UBVR difference photometry for N6946-BH1. The black circles indicate 'good' data, and the open circles indicate 'low-quality' data. The grey-shaded region shows the dispersion of the comparison sample. The vertical dashed line indicates the observed transient peak (2009-03-25). The comparison sample is contaminated by the transient near its peak, leading to a large dispersion at these epochs.

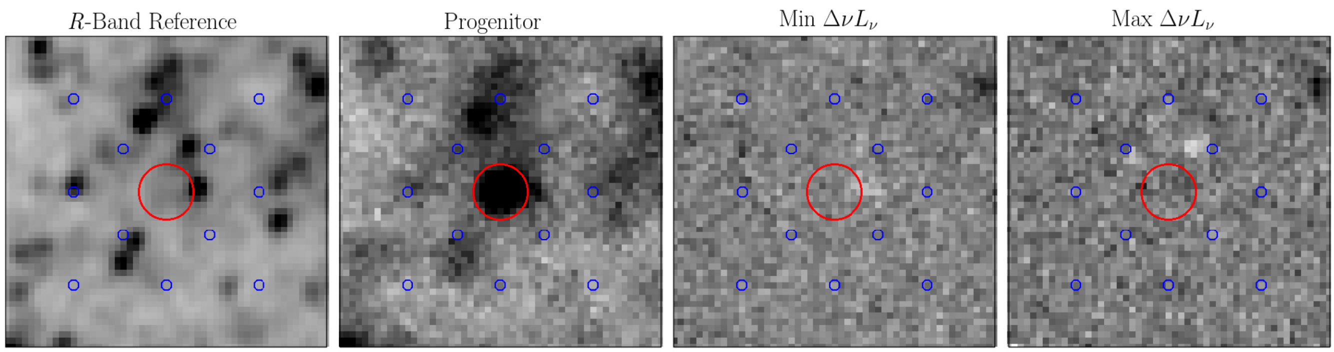

Figure 3. *R*-band images centred on the location of N6946-BH1. From left to right, the panels show the reference image, a pre-outburst image of the progenitor (2008-05-03), and two 'good' post-outburst difference images: the minimum luminosity (2013-12-03), and the maximum luminosity (2015-04-20). The scales of the difference images is symmetric about zero. The red circles are 1 arcsec in radius and are centred on N6946-BH1. The smaller blue circles indicate the positions used for the comparison sample. In all panels, darker colours indicate a greater flux.

has a slightly inflated value due to the contribution from 'low-quality' data points to the RMS (Fig. 2). We conclude that there is no evidence from the RMS for stochastic variability in the late-time light curve of N6946-BH1 at the level of $\sim 1000\,L_\odot$.

We also performed a linear fit, $L(t) = At + B$, to the post-outburst light curves to look for long-term trends in luminosity. This used data from epochs beginning with 2012 April 28, ensuring that sufficient time had passed for the transient to fade. The slopes in Table 2 are both positive and negative across the bands, and very close to $0\ L_\odot\ \mathrm{yr}^{-1}$. From the start date until 2019 October, the changes in luminosity are 700 ± 600, 1300 ± 1600, 300 ± 1000, and $-2400 \pm 1700\,L_\odot$ in the *R*, *V*, *B*, and *U* bands (corresponding to 2σ upper limits of 2000, 4500, 2400, and $1000\,L_\odot$). We also do linear fits to the points in the comparison sample and report the average absolute value of their slopes and their standard deviations in the second 'Sample' column in Table 2. The variability of N6946-BH1 is consistent with the comparison sample, with a slope close to zero that is consistent with the absence of any long-term trends.

4 CONSTRAINTS ON A SURVIVING STAR

If we adopt a range of temperature estimates for a surviving source and fit the new *HST* and *SST* near-IR and IR fluxes, we can determine the allowed luminosity of the source as a function of the temperature

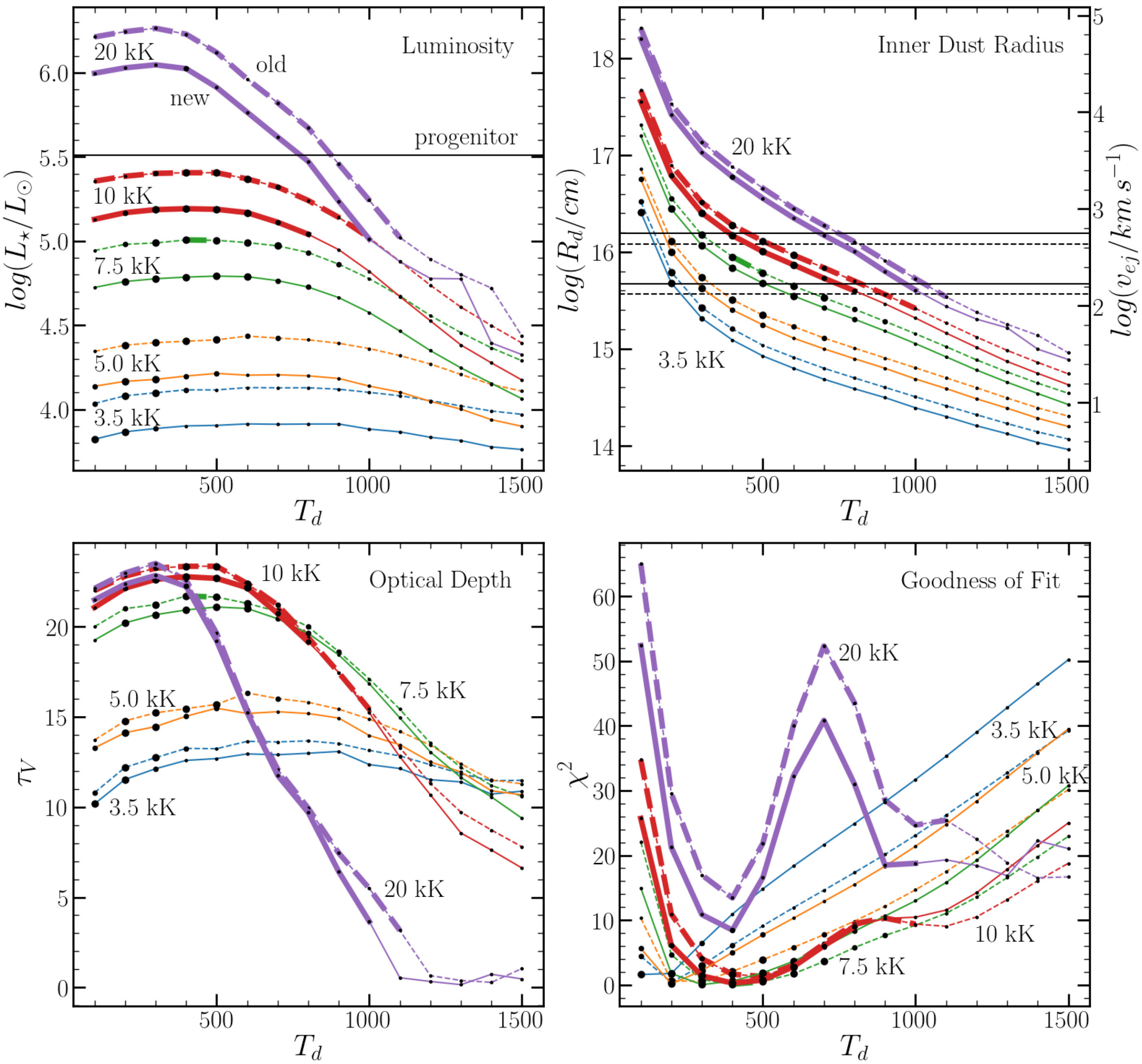

Figure 4. Parameters of the best-fitting models for a surviving source behind a dusty shell as a function of the dust temperatures (T_{d}, x-axis) at the inner edge of the shell. The upper left-hand panel shows the best-fitting luminosities of our models, the upper right-hand panel shows the best-fitting inner dust radii, the lower left-hand panel shows the best-fitting optical depths, and the lower right-hand panel shows the corresponding χ^2 values. Models for the old, 2015/2016 *HST*/*SST* measurements are shown with the dashed lines, while models for the more recent 2017/2018 *HST*/*SST* measurements are shown by the solid lines. Larger (smaller) black points indicate that the models fit better (worse). Each coloured curve corresponds to a constant stellar temperature, $T_\star$: Blue – 3500 K, Yellow – 5000 K, Green – 7500 K, Red – 10 000 K, and Purple – 20 000 K. The thicker curves indicate models with a luminosity $L_\star > 10^5\ \mathrm{L}_\odot$. In the upper left, the solid black line shows the luminosity of the progenitor. In the upper right, the solid (dashed) black lines corresponding to the new (old) measurements show the $170 < v_{\mathrm{ej}} < 560\ \mathrm{km\,s^{-1}}$ constraint on the ejecta velocity from Adams et al. (2017a).

Table 2. Variability limits.

Band	Variability ($10^3\ \mathrm{L}_\odot$)			Slope ($10^3\ \mathrm{L}_\odot\ \mathrm{yr}^{-1}$)	
	RMS	$\langle\sigma^2\rangle^{1/2}$	Sample	Late-time	Sample
R	0.9	0.6	0.8 ± 0.1	0.09 ± 0.08	0.04 ± 0.03
V	2.4	0.6	1.4 ± 0.2	0.18 ± 0.21	0.09 ± 0.04
B	1.6	0.9	1.6 ± 0.4	0.04 ± 0.14	0.10 ± 0.09
U	2.8	2.0	3.2 ± 0.5	-0.32 ± 0.23	0.20 ± 0.15

T_{d} of any surrounding dust. We do this using DUSTY (Ivezic & Elitzur 1997; Ivezic, Nenkova & Elitzur 1999; Elitzur, Ivezić & Ž. 2001), a radiative transfer code that models the light from a star surrounded by a spherical dusty shell or a dusty wind. As in Adams et al. (2017a), DUSTY is run inside a Markov Chain Monte Carlo wrapper to optimize the fits and to estimate uncertainties. Here, we only consider the case of a dusty shell as models with a dusty wind were previously ruled out in Adams et al. (2017a). Such models were too bright in the near/mid-IR due to the presence of hot dust.

For our models, we consider our 2015 *HST I*-band image to be an upper limit, as there was no coincident source in the optical, but we consider both our 2015 and 2017 *J*- and *H*-band images to be detections of the source in the near-IR. The latest *SST* channel 1 and channel 2 data points (2016 January 21 and 2018 September 20) are among the lowest observed IR measurements and are treated as upper limits due to the problems with aperture photometry in a crowded field given *SST*'s resolution. We only consider the case of silicate dust, which is the type of dust favoured to be formed from massive stars. The results will not strongly depend on whether we use silicate or graphitic dust.

We consider a range of stellar temperatures from $T_\star = 3500$–20 000 K. Adams et al. (2017a) noted that a temperature of 3500 K was likely for the progenitor. At each stellar temperature, we run a model with a fixed inner edge dust temperature T_d, ranging from 100 to 1500 K. The outer and inner dust radii are fixed to a ratio of 2.0 as it has little effect on the fits. With $T_\star$ and T_d fixed, the fits determine the visual optical depth of the shell τ_V and the luminosity of the star $L_\star$. We show the results of our fits in Fig. 4. The results for the 2015 *HST* and 2016 *SST* data are shown by the dashed lines, and the results for the 2017 *HST* and 2018 *SST* measurements are given by the solid lines. The thicker lines indicate a luminosity $L_\star > 10^5\,\mathrm{L}_\odot$. The size of the black points roughly indicates the quality of the fits, with larger points corresponding to smaller χ^2 values.

In the upper left of Fig. 4, we see that only hot stars ($T_\star \gtrsim 10\,000$ K) can have present-day luminosities similar to that of the progenitor ($\sim$300 000 $\mathrm{L}_\odot$, given by the black line). A star with a temperature similar to that of the progenitor ($T_\star \approx 3500$ K, the blue curve) must be far fainter. Because the near-IR emission has faded, the required temperature increases between the two *HST* epochs.

For ejecta velocities of $170 < v_\mathrm{ej} < 560\,\mathrm{km\,s^{-1}}$ (estimated by Adams et al. 2017a), the ejecta lie between the black lines at roughly $R_\mathrm{d} = 10^{16}$ cm. This allows the dust to be cool enough ($T_\mathrm{d} \sim 800$ K) to be invisible to warm *SST*. Note that the hot star solution with $T_\mathrm{d} \approx 800$ K fits badly because it struggles to keep the flux below the *SST* upper limits. Solutions with hotter dust require very slow expansion speeds and essentially approach a dusty wind model. Very cold dust generally requires very fast ejecta velocities and the large dust radii also require larger dust masses. Models with either very hot or very cold dust are generally bad fits.

In the lower left of Fig. 4, we see that the optical depths required to fit the new epochs are generally lower than those required to fit the SED in 2015/2016. If we adopt the epochs of the *HST* observations as the dates for the SEDs and 2008 Nov 25 as the date of the outburst, then the predicted change in the optical depth between the two observations for a t^{-2} scaling is $\tau_{\mathrm{V}_1} \approx 0.6\,\tau_{\mathrm{V}_0}$ since the observations were made 6.9 and 8.8 yr after the outburst. While the SED models do show small drops in the estimates of τ_V, typically to a fraction >0.9 of τ_{V_0}, the decrease is too small for an expanding shell over this time period. In fact, the observed drop is primarily driven by the lower luminosities found for the later epoch – the drop in the near-IR flux leads to lower-luminosity solutions that need less dust to keep the SED below the optical and mid-IR flux limits.

We can approximately correct for this effect by defining a luminosity-corrected optical depth for the second epoch of $\tau_{\mathrm{V}_1,\mathrm{corr}} \approx \tau_{\mathrm{V}_1} + \ln(L_0/L_1)$, where L_0/L_1 is the ratio of the luminosities between the two epochs. This correction is small, with an average ratio $\tau_{\mathrm{V}_1,\mathrm{corr}}/\tau_{\mathrm{V}_1} = 1.08$. Fig. 5 compares the corrected optical depth estimates (dashed lines) with the prediction for an expanding shell extrapolated from our first epoch (dotted lines). Both with and without the correction, the optical depths at the second epoch are too large to be consistent with the expected evolution of the optical depth between the two epochs.

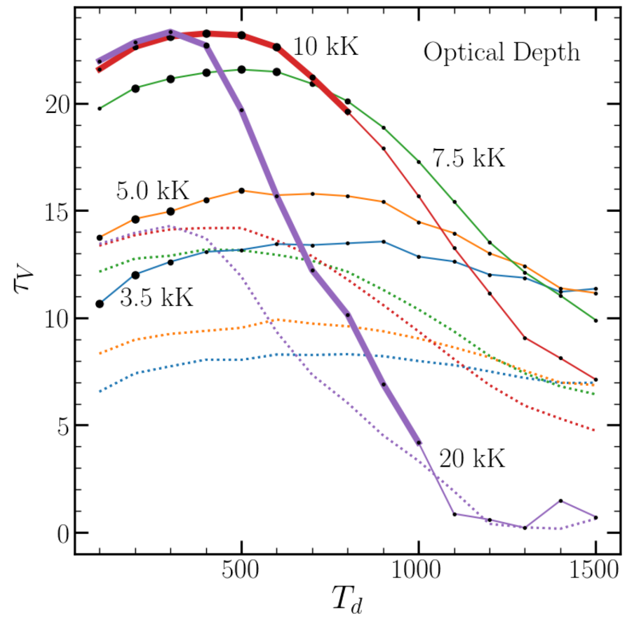

Figure 5. The corrected optical depths (solid lines) and expected optical depths (dotted lines). The corrected optical depth is defined as the optical depth required for the new measurements when the luminosity determined from the old measurements is held constant in our updated models. The expected optical depth follows a t^{-2} evolution between the two epochs. The colours of the curves indicate the effective stellar temperature, the thick curves indicate a luminosity $L_\star > 10^5\,\mathrm{L}_\odot$, and the sizes of the black points roughly correspond to the goodness of fit as in Fig. 4.

The optical depth can be roughly converted to an ejecta mass by $M_\mathrm{ej} = 4\pi R_\mathrm{d}^2 \tau_\mathrm{V}/\kappa_\mathrm{V}$ for a dust opacity scaled by $\kappa_\mathrm{V} = 100\mathrm{cm}^2\mathrm{g}^{-1}$. The ejecta mass is shown in Fig. 6, with the black line representing the Great Eruption of η Carinae for comparison (Humphreys & Davidson 1994; Humphreys, Davidson & Smith 1999). The newest measurements require a lower ejecta mass than the old measurements due to the decreasing $L_\star$ and R_d in the models of the new measurements with lower IR fluxes. Hiding the star requires an ejecta mass of ~ 0.1–$1(\kappa_\mathrm{V}/100\,\mathrm{cm}^2\,\mathrm{g}^{-1})^{-1}\,\mathrm{M}_\odot$ assuming a sufficiently hot star. While the lack of optical depth evolution is inconsistent with an expanding shell, the mass budget is still plausible given that it is much less than the total hydrogen envelope mass of $\sim 13\,\mathrm{M}_\odot$ for a $\sim 25\,\mathrm{M}_\odot$ red supergiant.

Based on the velocities and ejecta masses in Figs 4 and 6, we estimate the required ejecta energies with the results shown in Fig. 7. The black horizontal lines show the energy of a typical SN ($\sim 10^{51}$ erg), the kinetic energy of η Carinae's Great Eruption ($10^{48.8}$ erg, Davidson & Humphreys 1997), and an estimate for the luminous energy of the transient ($\sim 10^{47}$ erg). Plausible kinetic energies should be larger than the observed luminous energy.

For our calculations throughout this section, we computed the velocity, mass, and energy using the inner edge dust radius. If we instead consider the outer edge dust radius, we find a velocity and a mass that are two times larger, and an energy that is roughly five times larger. Such changes only strengthen our conclusions.

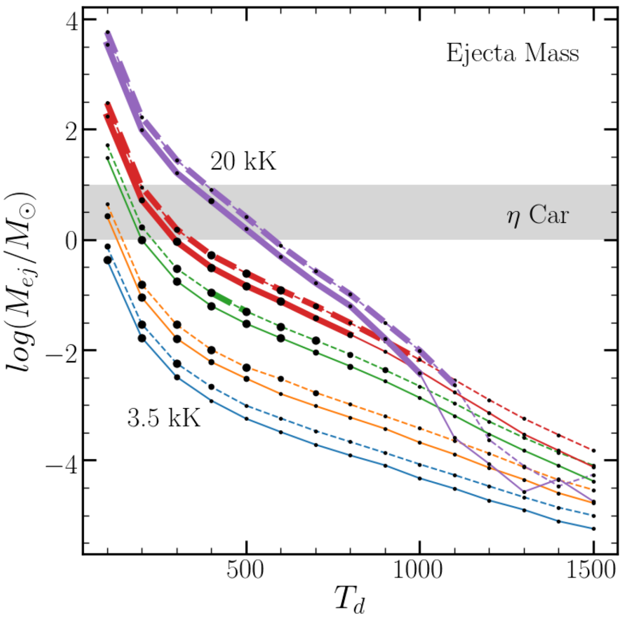

Figure 6. Ejecta mass $M_{\rm ej} = 4\pi R_{\rm d}^2 \tau_{\rm V}/\kappa_{\rm V}$ implied by the optical depth for an opacity of $\kappa_{\rm V} = 100\rm cm^2 g^{-1}$. The grey-shaded region shows a range of possible ejecta masses from η Carinae's Great Eruption. The colours of the curves indicate the effective stellar temperature, the thick curves indicate a luminosity $L_\star > 10^5\,\rm L_\odot$, and the sizes of the black points roughly correspond to the goodness of fit as in Fig. 4.

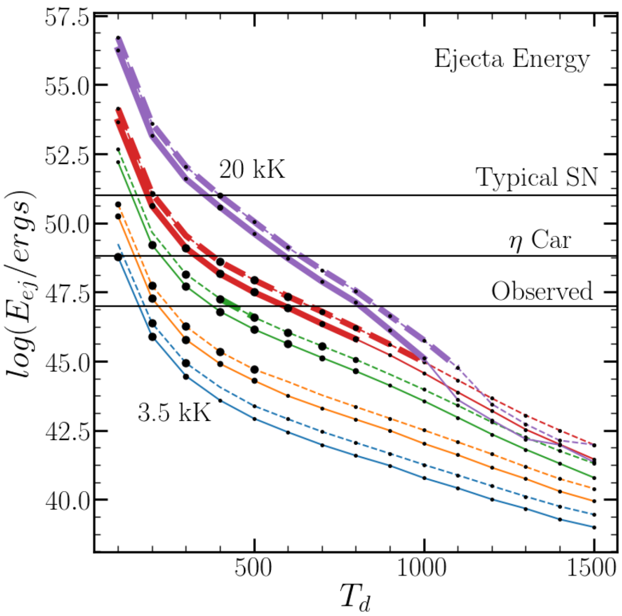

Figure 7. Energies required for the velocities and ejecta masses in Figs 4 and 6. The black horizontal lines show a typical SN energy, the kinetic energy of η Carinae's Great Eruption, and a rough estimate of the luminous energy of the observed transient. The colours of the curves indicate the effective stellar temperature, the thick curves indicate a luminosity $L_\star > 10^5\,\rm L_\odot$, and the sizes of the black points roughly correspond to the goodness of fit as in Fig. 4.

5 WHAT IS EXPECTED FOR A FAILED SN?

Fernández et al. (2018) were puzzled that Adams et al. (2017a) found a luminosity decay rate roughly as predicted in Perna et al. (2014) because their models predicted fall-back accretion on to the newly formed black hole that was super-Eddington for an extended period of time (decades). Assuming the actual emission is Eddington-limited, this would suggest that a failed SN should initially have a roughly constant luminosity of the same magnitude as the luminosity of the progenitor since the Eddington limit for a 10 $\rm M_\odot$ black hole is 330 000 $\rm L_\odot$. Since Kochanek (2014b) showed that the ejected stellar envelope of a failed SN would form dust very efficiently, it would seem that the emission from a failed SN would produce almost the same scenario as we have discussed for limiting the properties of a surviving star in Section 4. It appears to be the same scenario until the accretion drops, although the time-scales for the dust clearing would be longer (see below) than our current observation period because of the large ejecta mass ($\sim 10\,\rm M_\odot$) and modest velocities ($\sim$200 km s^{-1}).

There is, however, a fundamental difference between the SED of a star and that of an accreting, stellar mass black hole – temperature. The characteristic temperature for the inner edge of a thin accretion disc around an Eddington-limited 10 $\rm M_\odot$ Schwarzschild black hole is $T_{\rm in} \simeq 3 \times 10^7$ K or 2.3 keV, which is why X-rays are a primary focus of black hole binary studies (see e.g. the review by McClintock & Remillard 2006). For a Shakura & Sunyaev (1973) thin disc with this temperature at the inner edge, the fraction of the disc luminosity emitted longwards of 0.1 µm, still well into the UV, is $\sim 10^{-3}$. The fraction emitted in the near-IR longwards of 1 µm is 4×10^{-5}. The actual fraction can be higher due to additional radiative processes or jets, but one should not expect much direct emission from the accreting black hole in the optical or near-IR. Thus, while the the expansion of the ejecta still eventually clears the veil of dust to reveal any central source, in an accretion scenario there is not much of a central source to reveal in the optical and near-IR.

The newly formed black hole is still surrounded by the ejected envelope of the red giant, and the envelope will absorb the X-rays as discussed in Section 2 for the *Chandra* observations. At 2 keV, the X-ray opacity is $\kappa \simeq 15\ \rm cm^2\,g^{-1}$(Draine & Woods 1991), so 10 $\rm M_\odot$ of ejecta moving at 200 km s^{-1} would remain optically thick for over two centuries. The X-rays are, however, absorbed by the gas and not the dust (i.e. for X-rays, the gas opacity is greater than the dust opacity) with two consequences. First, it is an expanding flow, so there are *PdV* losses of energy into expansion. For a constant velocity expansion, 2/3 of the energy goes into expansion and only 1/3 goes into heating the gas. Because the ejected envelope is already expanding rapidly, there is little acceleration and the constant velocity limit is valid. As a result, the net luminosity which will ultimately be radiated is reduced by a factor of 3.

The second consequence of the temperature difference is that the energy is deposited in a thicker layer of the ejecta because keV X-ray opacities are less than optical/ultraviolet dust opacities. Since the ejecta should still be optically thick in dust, the radiated energy will still ultimately emerge as emission from grains. The X-rays heat the gas, collisions with the gas and absorption of optical/ultraviolet radiation from atomic lines and recombination heat the dust, and then the dust produces the radiation which can ultimately escape. However, since the X-rays heat the gas in a larger volume containing more dust grains because of the lower opacity than in the optical, the grain temperatures will be reduced and the dust emission will shift to longer wavelengths than the stellar scenarios considered in Section 4. The details of these radiative processes are complex (they are certainly beyond the capabilities of DUSTY) and a more detailed/quantitative discussion is beyond the scope of this paper.

How then is the declining near-IR emission to be interpreted under the failed SN interpretation? It does seem clear that simply following Adams et al. (2017a) and interpreting it as the accretion luminosity decay predicted in Perna et al. (2014) is likely untenable. However, it is also clear that the concern in Fernández et al. (2018) that one should be seeing luminosity corresponding to Eddington-limited accretion is also untenable. It does seem likely that there should be longer wavelength mid-IR emission at something like 1/3 of the accretion luminosity that could be observed with the *JWST*. It also seems at least plausible that there may be a hot dust tail to this emission which decays as the ejecta expands and it becomes more difficult to have any hot dust, but this is largely just speculation.

6 SUMMARY

We present new LBT, *HST*, and *SST* data for our failed SN candidate in NGC 6946. Investigation of the LBT light curve finds no evidence for either variability or long-term trends in the luminosity of any possible surviving star with an upper limit of 2000 $L_\odot$ for any re-brightening of the *R*-band luminosity. *HST* and *SST* observations in 2017/2018 show that the source has faded by nearly a factor of 2 in the near/mid-IR since the 2015/2016 epochs.

Using our *HST* and *SST* observations, we create SED models for a potential surviving source surrounded by a spherical shell of dust. In the most recent *HST* and *SST* data, lower luminosity sources are more favoured given the apparent decline in flux. To hide a $\sim$300 000 $L_\odot$ star like the progenitor, our models require a much higher effective stellar temperature ($T_\star \gtrsim 10\,000$ K) for a surviving source. Otherwise, a star with similar effective temperature to the progenitor ($\sim$ 3500 K) must be intrinsically much fainter. However, the most intriguing result from these models is the requirement for minimal evolution of the optical depth between the two epochs under the assumption of a surviving star, which does not match the behaviour of an expanding dusty shell. While surviving stars with the appropriate properties can fit the instantaneous SEDs, the lack of optical depth evolution between the two epochs rules out these models. Obscuration by an ongoing wind remains ruled out by the new data.

The requirement that the optical depth drops with time is a physical necessity for any model using a cool dust shell to hide the star. We know that the progenitor was little obscured, so the present obscuration must be due to dust newly formed in the transient. For that dust to be cool today, it has to have expanded away from the star at several 10^2–10^3 km s^{-1}. Once it is in expansion, it must continue to expand, and if it continues to expand, the optical depth must drop at least as fast as t^{-2}. Because dust growth is collisional, the dust properties are frozen early in the evolution, and the opacity now is constant while the surface density is dropping. As discussed in the introduction, this minimal t^{-2} scaling of the optical depth is simply a consequence of mass conservation and not specific to our spherical models. Any development of inhomogeneities in the shell accelerates the evolution, essentially because photons start to escape more easily through lower optical depth paths, so assuming a t^{-2} optical depth evolution is a conservative assumption.

We also searched for X-ray emission with *Chandra*, which would be produced by fallback accretion on to a black hole. This unsuccessful attempt set an upper limit on the luminosity of an accreting, 10 $M_\odot$ black hole at $4.2 \times 10^{-3} L_{\rm E}$. If such a black hole were radiating at the Eddington limit in X-rays, the observing limit would be met given an obscuring column of N(H) $\gtrsim 10^{24}$cm^{-2}, roughly corresponding to an ejecta mass of $\gtrsim 1\,M_\odot$ that would be easily exceeded by a failed SN of a $\sim 25\,M_\odot$ star with $13\,M_\odot$ of ejecta.

We know of no other massive, luminous star which has been so dust enshrouded for so long. η Carinae is probably the one known example of a star that remained optically faint relative to its progenitor for an extended period. In the 1800s, η Carinae erupted and then dimmed and remained visually dim for decades (see Humphreys & Davidson 1994; Humphreys et al. 1999). Following its second outburst, its luminosity remained relatively constant at a few per cent of its initial luminosity before gradually beginning to re-brighten in the mid 1900s. Its rate of luminosity change in the late 1800s was probably close to the limits we find here. However, there are two problems with this analogue as an explanation for N6946-BH1. First, η Carinae would have been a tremendously luminous warm-*Spitzer* source for this entire period, easily seen in any nearby galaxy like NGC 6946 (see Khan et al. 2010; Khan, Stanek & Kochanek 2013) and thereby easily ruled out as a failed SN. Secondly, η Carinae's evolutionary time-scales including its outburst were decades, while the outburst time-scale of N6946-BH1 was less than a year. This would suggest that the 'recovery' time-scale for this system should also be far faster than observed for η Carinae and even moderately compressing the evolution of η Carinae implies brightness changes which we would have easily observed.

Our candidate remains at a luminosity of $\sim$1 per cent of its progenitor, and we have not detected re-brightening nearly a decade after the initial outburst. In the failed SN scenario, the current luminosities may be explained as radiation from hot dust that is heated by X-rays produced from a hot accretion disc. The X-rays heat the gas in the ejected envelope, collisions with the gas and absorption from re-radiated photons heat the dust formed in the ejecta (Kochanek 2014b), and then the dust re-radiates the photons which ultimately escape. In detail, the radiative and heating processes are much more complex than the dust equilibrium radiative transport models we can use for a surviving star, and further studies are needed of expected observables for failed SNe. Because a disc radiates predominantly X-rays, there is no luminous optical/near-IR source to be revealed as the dust optical depth drops. In the meantime, continued optical and near-IR monitoring is one means of showing there is no surviving dust-obscured star. It is, however, a somewhat indirect method. After *JWST* launches, 10-20 μm observations can directly test the possibility that a luminous star is hidden in cooler dust than can be detected with *SST* observations. For now, N6946-BH1 remains an excellent failed SN candidate with no compelling alternative explanation.

ACKNOWLEDGEMENTS

We thank Rachel Patton for her assistance with DOLPHOT photometry. CSK and KZS are supported by NSF grants AST-1814440 and AST-1908952. Based on observations made with the NASA/ESA *Hubble Space Telescope*, obtained from the Data Archive at the Space Telescope Science Institute, which is operated by the Association of Universities for Research in Astronomy, Inc., under NASA contract NAS5-26555. These observations are associated with programs GO-14266 and GO-15312. This work is based in part on observations made with the *SST*, which is operated by the Jet Propulsion Laboratory, California Institute of Technology under a contract with NASA. The LBT is an international collaboration among institutions in the United States, Italy and Germany. LBT Corporation partners are as follows: The University of Arizona on behalf of the Arizona Board of Regents; Istituto Nazionale di Astrofisica, Italy; LBT Beteiligungsgesellschaft, Germany, representing the Max-Planck

Society, The Leibniz Institute for Astrophysics Potsdam, and Heidelberg University; The Ohio State University, representing OSU, University of Notre Dame, University of Minnesota and University of Virginia. Support for this work was provided by the National Aeronautics and Space Administration through *Chandra* Award Number 17500057 issued by the *Chandra* X-ray Center, which is operated by the Smithsonian Astrophysical Observatory for and on behalf of the National Aeronautics and Space Administration under contract NAS8-03060.

DATA AVAILABILITY

The *HST*, *Chandra*, and *SST* data are available from the appropriate archives. The relevant LBT data are available by requesting them from the authors.

REFERENCES

Abbott B. P. et al., 2016, Phys. Rev. Lett., 116, 061102
Adams S. M., Kochanek C. S., 2015, MNRAS, 452, 2195
Adams S. M., Kochanek C. S., Beacom J. F., Vagins M. R., Stanek K. Z., 2013, ApJ, 778, 164
Adams S. M., Kochanek C. S., Gerke J. R., Stanek K. Z., Dai X., 2017, MNRAS, 468, 4968
Adams S. M., Kochanek C. S., Gerke J. R., Stanek K. Z., 2017, MNRAS, 469, 1445
Alard C., 2000, A&AS, 144, 363
Alard C., Lupton R. H., 1998, ApJ, 503, 325
Anand G. S., Rizzi L., Tully R. B., 2018, AJ, 156, 105
Belczynski K., Repetto S., Holz D. E., O'Shaughnessy R., Bulik T., Berti E., Fryer C., Dominik M.,2016, ApJ, 819, 108
Davidson K., Humphreys R. M., 1997, ARA&A, 35, 1
Dolphin A. E., 2000, PASP, 112, 1383
Draine B. T., Woods D. T., 1991, ApJ, 383, 621
Elitzur M., Ivezić Ž., 2001, MNRAS, 327, 403
Fernández R., Quataert E., Kashiyama K., Coughlin E. R., 2018, MNRAS, 476, 2366
Garmire G. P., Bautz M. W., Ford P. G., Nousek J. A., Ricker G. R., 2003, in Truemper J. E., Tananbaum H. D., eds, Proc. SPIE Conf. Ser. Vol. 4851, X-Ray and Gamma-Ray Telescopes and Instruments for Astronomy. SPIE, Belliongham, p. 28
Gerke J. R., Kochanek C. S., Stanek K. Z., 2015, MNRAS, 450, 3289
Holt S. S., Schlegel E. M., Hwang U., Petre R., 2003, ApJ, 588, 792
Humphreys R. M., Davidson K., 1994, PASP, 106, 1025
Humphreys R. M., Davidson K., Smith N., 1999, PASP, 111, 1124
Ivezic Z., Elitzur M., 1997, MNRAS, 287, 799
Ivezic Z., Nenkova M., Elitzur M., 1999, preprint (arXiv:astro-ph/9910475)
Johnson S. A., Kochanek C. S., Adams S. M., 2017, MNRAS, 472, 3115
Khan R., Stanek K. Z., Prieto J. L., Kochanek C. S., Thompson T. A., Beacom J. F., 2010, ApJ, 715, 1094
Khan R., Stanek K. Z., Kochanek C. S., 2013, ApJ, 767, 52
Kochanek C. S., 2014a, MNRAS, 444, 2043
Kochanek C. S., 2014b, ApJ, 785, 28
Kochanek C. S., 2015, MNRAS, 446, 1213
Kochanek C. S., Beacom J. F., Kistler M. D., Prieto J. L., Stanek K. Z., Thompson T. A., Yüksel H., 2008, ApJ, 684, 1336
Kochanek C. S., Szczygieł D. M., Stanek K. Z., 2012, ApJ, 758, 142
Lovegrove E., Woosley S. E., 2013, ApJ, 769, 109
McClintock J. E., Remillard R. A., 2006, in Lewin W., van der Klis M., eds, Compact stellar X-ray sources. Cambridge Univ. Press, Cambridge, p. 157
O'Connor E., Ott C. D., 2011, ApJ, 730, 70
Pejcha O., Thompson T. A., 2015, ApJ, 801, 90
Perna R., Duffell P., Cantiello M., MacFadyen A. I., 2014, ApJ, 781, 119
Schlafly E. F., Finkbeiner D. P., 2011, ApJ, 737, 103
Schlegel D. J., Finkbeiner D. P., Davis M., 1998, ApJ, 500, 525
Shakura N. I., Sunyaev R. A., 1973, A&A, 500, 33
Shappee B. J., Kochanek C. S., Stanek K. Z., 2013, ApJ, 765, 150
Smartt S. J., Eldridge J. J., Crockett R. M., Maund J. R., 2009, MNRAS, 395, 1409
Sukhbold T., Ertl T., Woosley S. E., Brown J. M., Janka H.-T., 2016, ApJ, 821, 38
Thompson T. A. et al., 2019, Science, 366, 637
Weisskopf M. C., Brinkman B., Canizares C., Garmire G., Murray S., Van Speybroeck L. P., 2002, PASP, 114, 1
Woosley S. E., Heger A., Weaver T. A., 2002, Rev. Mod. Phys., 74, 1015

This paper has been typeset from a TEX/LATEX file prepared by the author.